Journal of Solid State Chemistry 183 (2010) 2576–2581

Contents lists available at ScienceDirect

Journal of Solid State Chemistry

journal homepage: www.elsevier.com/locate/jssc

Hydrothermal synthesis and electrochemical performance of NiO microspheres with different nanoscale building blocks

Ling Wang, Yanjing Hao, Yan Zhao, Qiongyu Lai *, Xiaoyun Xu

College of Chemistry, Sichuan University, Chengdu 610064, PR China

ARTICLE INFO

Article history:
Received 1 June 2010
Received in revised form
20 August 2010
Accepted 1 September 2010
Available online 8 September 2010

Keywords:
NiO microsphere
Morphology
Growth mechanism
Electrochemical performance

ABSTRACT

NiO microspheres were successfully obtained by calcining the $Ni(OH)_2$ precursor, which were synthesized via the hydrothermal reaction of nickel chloride, glucose and ammonia. The products were characterized by TGA, XRD and SEM. The influences of glucose and reaction temperature on the morphologies of NiO samples were investigated. Moreover, the possible growth mechanism for the spherical morphology was proposed. The charge/discharge test showed that the as-prepared NiO microspheres composed of nanoparticles can serve as an ideal electrode material for supercapacitor due to the spherical hollow structure.

1. Introduction

The synthesis of inorganic nanomaterials with well-controlled morphologies has attracted considerable interest in recent years because the properties of these materials extensively depend on their size and shape [1–5]. NiO as an important transition metal oxide has received extensive attention because of its specific structure and potential applications in various fields, such as catalyst [6–8], battery cathodes [9], gas sensor materials [10], electrochromic films [11] and fuel cell electrodes [12,13]. It is well known that the properties and applications of NiO are closely related to its morphology, therefore, the synthesis of NiO with different size and shape has an important significance in fundamental science and practical application. Up to now, NiO with various morphologies has been prepared, such as nanoparticles [14], nanorods/nanowires/nanofibers [15–18], nanosheets [19], nanotubes [20], flower-like structures [21], hollow spheres [22] and nanosheet-based NiO microspheres [23]. However, there are few reports about NiO microspheres with different building blocks used in electrochemical capacitors.

In this paper, a facile method is used to synthesize NiO microspheres with different nanoscale building blocks via a hydrothermal route. The influences of glucose and reaction temperature on the morphologies of NiO samples were investigated. Moreover, the possible growth mechanism for the spherical morphology was proposed. The electrochemical performance of the NiO microspheres with different nanoscale building blocks was also investigated. In comparison with microspheres composed of nanoplates and microspheres with smooth surface, the NiO hollow microspheres composed of nanoparticles showed the best electrochemical performance.

2. Experimental section

2.1. Preparation of NiO microspheres

All the chemicals were purchased and used as received without any purification. In a typical synthesis of NiO hollow spheres experiment, 0.5348 g of $NiCl_2 \cdot 6H_2O$ and 0.2 mL of ammonia were dissolved in 19.8 mL of distilled water. Then, 2.0000 g of glucose was added and the mixed solution was stirring for 5 min. The resulting solution was transferred to a 25 mL Teflon-lined stainless-steel autoclave and heated at 140 °C for 12 h, and then cooled naturally to the room temperature. The product was collected by filtration, washed with distilled water and absolute ethyl alcohol. After the product was dried at 60 °C for 6 h, the black powder precursor was obtained. NiO hollow spheres could be acquired by calcining the obtained precursor at 450 °C for 2 h.

NiO microspheres with smooth surface can be prepared when the hydrothermal reaction temperature is up to 180 °C. NiO microspheres composed of nanoplates can also be obtained under the same reaction conditions and without glucose.

* Corresponding author. Fax: +86 28 85416969.
E-mail address: laiqy5@hotmail.com (Q. Lai).

0022-4596/$ - see front matter © 2010 Elsevier Inc. All rights reserved.
doi:10.1016/j.jssc.2010.09.006

2.2. Characterization

TGA was performed on a NETZSCH TG 209 F1 thermogravimetric analyzer with 50 mL/min of air flow from 50 to 600 °C at a heating rate 10 °C/min. Powder X-ray diffraction data were collected on a Rigaku D/MAX-rA diffractometer with Cu $K\alpha$ radiation (λ=0.15418 nm) being operated at 40 kV and 100 mA. The morphology and particle size were examined by the scanning electron microscope (SEM, JSM-5900LV, Japan).

2.3. Electrochemical measurements

Nickel oxide electrodes were prepared by pressing an active paste onto a nickel foam substrate. The paste contained 70 wt% as-obtained nickel oxide, 25 wt% acetylene black (AB) and 5 wt% polyvinylidene fluoride (PVDF), which were dissolved by N-methy-l-2-pyrrolidine (NMP). First, the paste was dried in vacuum at 60 °C for 12 h. Second, the active paste was pressed onto a nickel foam substrate that served as a current collector (surface was 1 cm^2) under a pressure of 20 MPa. Then the nickel oxide electrodes were dried in vacuum at 60 °C for 3 h.

The charge/discharge test was performed with a two-electrode cell in which the NiO electrode was used as positive electrode and the AC electrode was used as negative electrode in 6 mol/L KOH aqueous solutions, and it was carried out with Neware battery program-control testing system. All the charge/discharge tests were carried out at room temperature.

3. Results and discussion

3.1. Thermal analysis

TGA curve of the $Ni(OH)_2$ precursor is shown in Fig. 1. The initial weight loss of about 8% between 50 and 200 °C was due to the removal of physically adsorbed water molecules and carbonaceous polysaccharide. The rapid weight loss of about 90% between 200 and 450 °C corresponded to the removal of the intercalated water molecules and the decomposition of the $Ni(OH)_2$. Beyond 450 °C, all the intercalated water molecules and organic species were completely removed from the interslab space of $Ni(OH)_2$, and NiO was formed as the final product. Based on the thermal analysis, NiO can be prepared by calcining the $Ni(OH)_2$ precursor at 450 °C for 2 h.

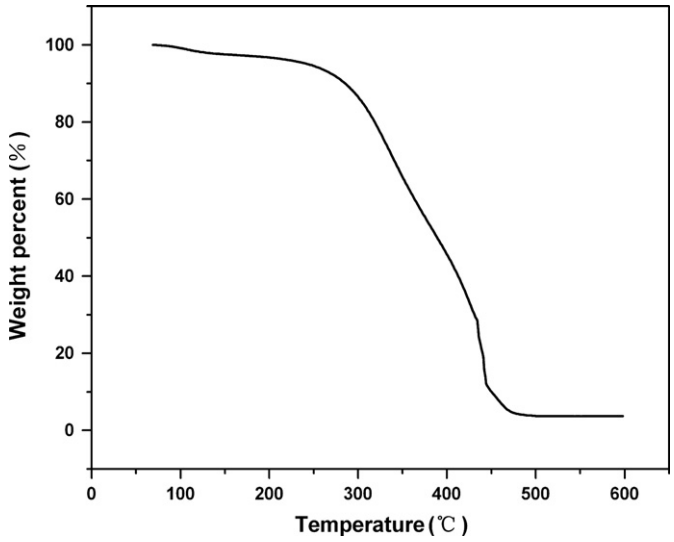

Fig. 1. TGA curve of $Ni(OH)_2$ precursor obtained at 140 °C for 12 h.

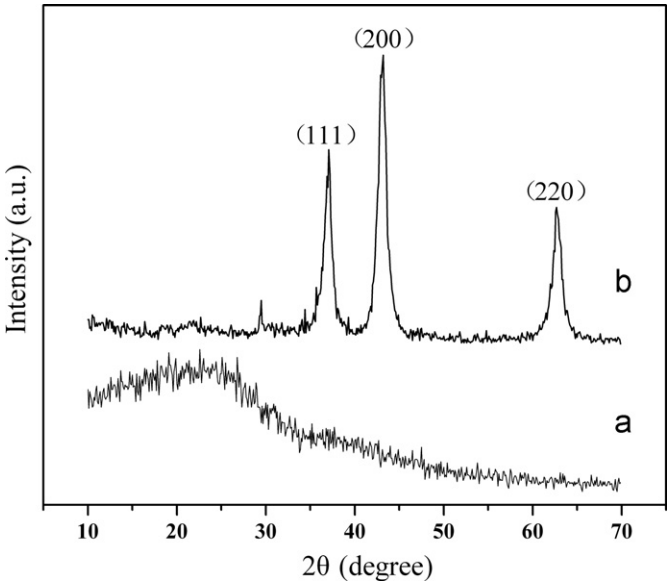

Fig. 2. (a) XRD pattern of $Ni(OH)_2$ precursor prepared in the present of glucose at 140 °C for 12 h and (b) XRD pattern of NiO sample after calcination $Ni(OH)_2$ precursor at 450 °C for 2 h.

3.2. XRD analysis

The XRD pattern of the $Ni(OH)_2$ precursor is presented in Fig. 2a. The broad diffraction peak indicates that the $Ni(OH)_2$ precursor has a poor crystallinity. Fig. 2b shows the XRD pattern of NiO sample after calcining $Ni(OH)_2$ precursor at 450 °C for 2 h. The diffraction peaks at 37.2°, 43.3° and 62.9° of 2θ are corresponding to the (1 1 1), (2 0 0) and (2 2 0) planes, respectively, which can be indexed perfectly to cubic NiO phase. These results are in good agreement with the data of JCPDS file No. 47-1049. It is clear that the resulting sample possesses very good crystallinity after it was annealed at 450 °C for 2 h.

Fig. 3 shows the XRD patterns of NiO samples obtained by calcining $Ni(OH)_2$ precursors prepared under the different hydrothermal conditions: in the presence of glucose at 140 °C for 12 h (Fig. 3a), without glucose at 140 °C for 12 h (Fig. 3b) and in the presence of glucose at 180 °C for 12 h (Fig. 3c). All the peaks in the XRD patterns can be indexed as the cubic pure phase of NiO (JCPDS No. 47-1049). No other peaks can be observed, indicating the high purity of the as-prepared NiO samples.

3.3. SEM analysis

Fig. 4a shows the SEM image of $Ni(OH)_2$ precursor obtained in the presence of glucose at 140 °C for 12 h. The $Ni(OH)_2$ precursor exhibits a spherical morphology with the diameter of 4–5 μm and the sphere surface is relatively smooth. SEM image of NiO hollow microspheres obtained by calcining $Ni(OH)_2$ precursor at 450 °C for 2 h is shown in Fig. 4b. The NiO hollow microsphere has an average diameter of 2 μm and an average shell thickness around 200 nm. The obvious holes found on NiO hollow spheres were produced by the rapid combustion process. Under the fast calcination process, the gas produced by burning carbonaceous polysaccharide was rapidly released, leading to the appearance of holes. Such porous structure had much more specific surface area than that of compact structure, which was expected to exhibit better properties in electrochemistry.

We found that the reaction temperature played a crucial role in the formation of the products. Fig. 5 shows the SEM images of $Ni(OH)_2$ and NiO samples synthesized at different reaction temperatures. At the reaction temperature of 80 °C (Fig. 5a), only nanoparticles could be prepared. After calcining at 450 °C for 2 h, the nanoparticles were aggregated and formed large particles (Fig. 5b). When the reaction temperature was up to 140 °C, the sample morphologies changed and spherical $Ni(OH)_2$ samples with a diameter of 4–5 μm were prepared (Fig. 5c). The NiO hollow spheres with an average diameter of 2 μm were obtained after fast calcination at 450 °C for 2 h (Fig. 5d). The holes existed on the rough surface of hollow spheres can be obviously observed. At the higher temperature of 180 °C, $Ni(OH)_2$ microspheres with smooth surface appeared as the main products (Fig. 5e). From Fig. 5f we can see that NiO microspheres with smooth surface were obtained, indicating the spherical morphology can be well sustained after the heat treatment process.

In addition, glucose also played an important role in the formation of the hollow microsphere composed of nanoparticles. Fig. 6a and c shows the SEM images of $Ni(OH)_2$ samples prepared without glucose. The $Ni(OH)_2$ samples have sphere-like morphologies, which are composed of many nanoplates. After calcining at 450 °C for 2 h, the spherical morphology was still retained (Fig. 6c and d). However, the tightness of NiO spherical aggregation was increased.

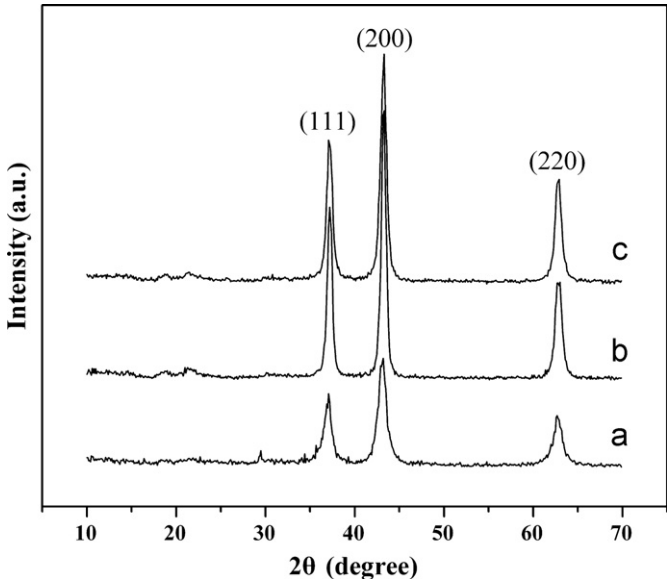

Fig. 3. XRD patterns of NiO obtained by calcining $Ni(OH)_2$ precursors prepared in the different hydrothermal conditions: (a) adding glucose, 140 °C 12 h (b) without glucose, 140 °C 12 h and (c) adding glucose, 180 °C 12 h.

3.4. Formation mechanism of NiO microspheres

Taking into account the contributions of Sun and Li [24], Li et al. [25] and Titirici et al. [26], the possible growth mechanism for NiO hollow sphere was proposed. When the mixture of $NiCl_2 \cdot 6H_2O$, ammonia and glucose were treated at 140 °C under hydrothermal conditions, carbonaceous polysaccharide microspheres were formed and their surface had a large number of hydroxyl and carbonyl groups with good hydrophilicity. Ni^{2+} ions would adsorb on the surface of carbonaceous polysaccharide microspheres and simultaneously react with OH^- ions provided by the hydrolysis of the ammonia, which resulted in the formation of an incompact nickel hydroxide shell. NiO hollow sphere could be easily achieved by a rapid combustion process. When the hydrothermal reaction temperature increased up to 180 °C, the hydrolysis of the ammonia provided more OH^- ions. Ni^{2+} cations reacted with more OH^- ions to form nickel hydroxide shell. The thickness of the nickel hydroxide was larger than that of nickel hydroxide obtained at 140 °C. The spherical morphology with a smooth surface could be sustained by a rapid heat treatment process. From the XRD patterns of Fig. 3a and c, it should be noted that the sample synthesized at 180 °C has stronger diffraction intensity and narrower half-peak width, indicating the product synthesized at this temperature has a higher crystallinity. Hence, the complete and smooth surface microsphere was obtained at 180 °C.

It is well known that $Ni(OH)_2$ has a hexagonal layer structure. Under a certain hydrothermal condition (without glucose, at 140 °C for 12 h), $Ni(OH)_2$ nanoplatelets are easily formed because of their intrinsic lamellar structure. The nanoplatelets can aggregate into the spherical morphology through self-assembly process by the driving forces, such as electrostatic and dipolar fields associated with the aggregation, hydrophobic interactions, hydrogen bonds, crystal-face attraction and van der Waals forces [27]. The spherical morphology composed of nanoplates can be sustained by a rapid heat treatment process.

3.5. Electrochemical performance of the products

To investigate the effect of different morphologies of NiO on the electrochemical properties, their charge/discharge performances were measured.

The NiO microsphere samples prepared by calcining the $Ni(OH)_2$ precursor at 450 °C for 2 h were used as electrode material for charge/discharge test. Figs. 7 and 8 show the

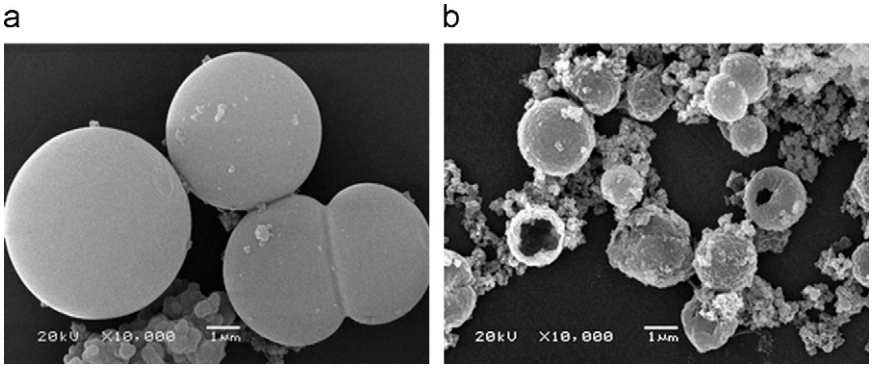

Fig. 4. (a) SEM image of $Ni(OH)_2$ precursors obtained in the present of glucose at 140 °C for 12 h and (b) SEM image of NiO hollow microspheres obtained by calcining $Ni(OH)_2$ precursors at 450 °C for 2 h.

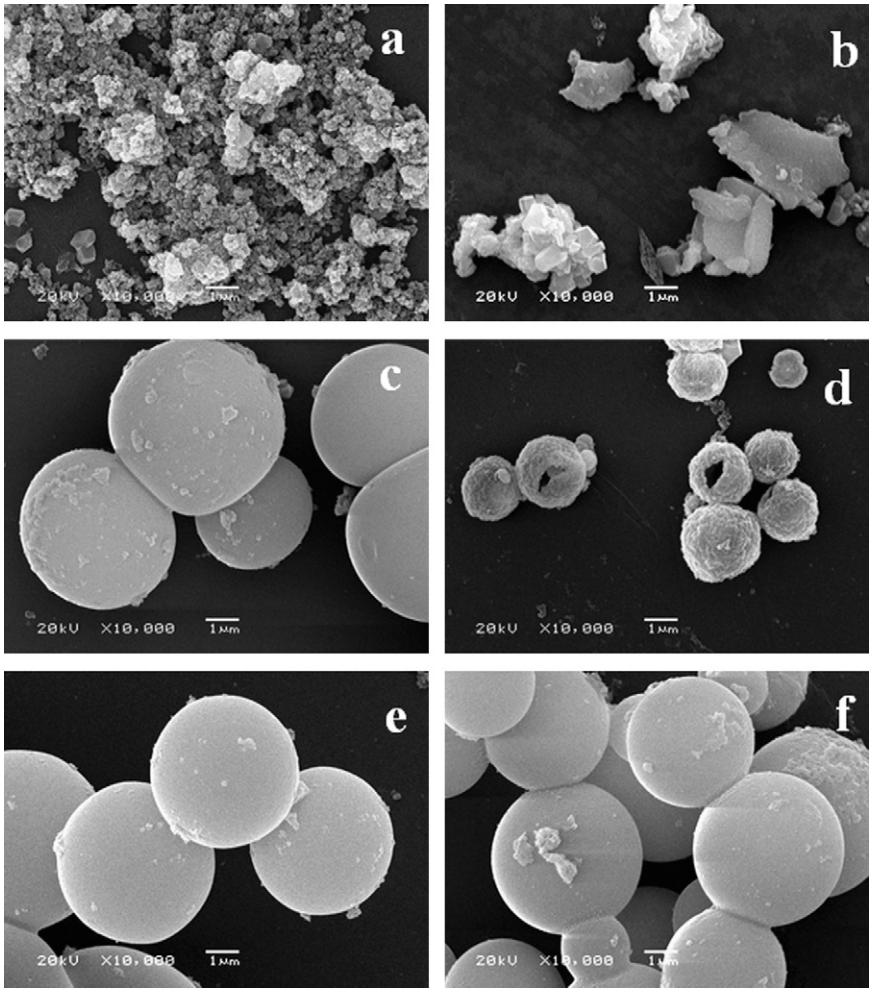

Fig. 5. SEM images of $Ni(OH)_2$ (left-hand) and NiO (right-hand) samples obtained at various reaction temperatures: (a, b) 80 °C, (c, d) 140 °C and (e, f) 180 °C.

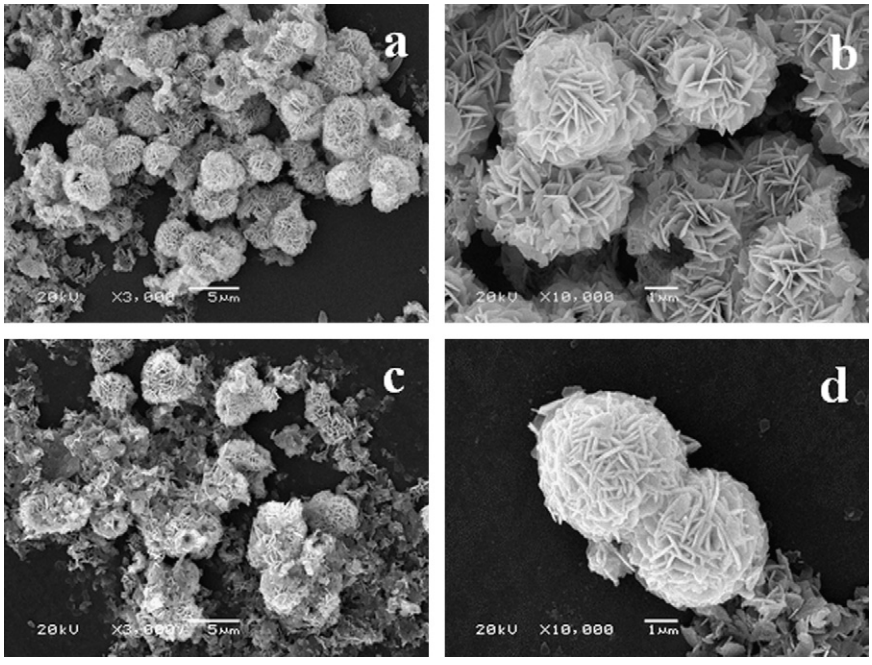

Fig. 6. (a) SEM image of $Ni(OH)_2$ samples obtained without glucose at 140 °C for 12 h, (c) NiO samples obtained after calcining at 450 °C for 2 h, (b) and (d) the magnification images of the photographs of (a) and (c), respectively.

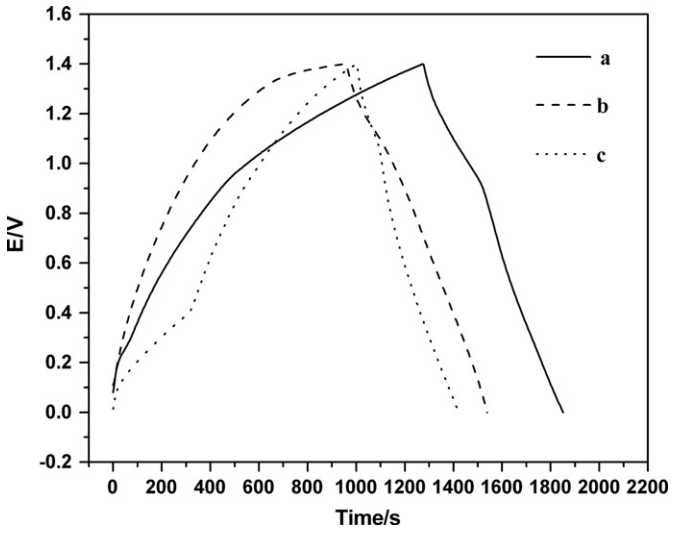

Fig. 7. The charge/discharge curves of the first cycle for the NiO/AC supercapacitor at a constant current density of 100 mA/g in 6 mol/L KOH solution: (a) NiO hollow sphere composed of nanoparticles, (b) NiO sphere composed of nanoplates and (c) NiO sphere with a smooth surface.

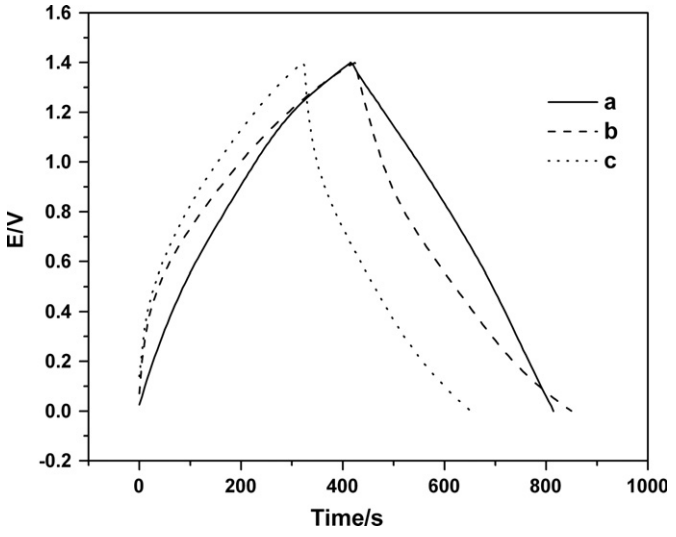

Fig. 8. The charge/discharge curves of the 1000th cycle for the NiO/AC supercapacitor at a constant current density of 100 mA/g in 6 mol/L KOH solution: (a) NiO hollow sphere composed of nanoparticles, (b) NiO sphere composed of nanoplates and (c) NiO sphere with a smooth surface.

charge/discharge curves of the first and the 1000th for the NiO/AC supercapacitor at a constant current density of 100 mA/g in 6 mol/L KOH solution, respectively. As shown, a good linear potential variation vs. time is observed for all charge/discharge curves, which is a typical characteristic of an ideal supercapacitor. The charge-storage mechanism of NiO for a pseudo-capacitor electrode in alkaline solution has been represented as an invertible oxidation–reduction reaction between Ni^{2+} and Ni^{3+}, which is described by the following reaction [28]:

$$\mathrm{Nio} + z\mathrm{OH}^- \underset{\text{discharge}}{\overset{\text{charge}}{\rightleftharpoons}} z\mathrm{NiOOH} + (1-z)\mathrm{NiO} + ze^- \quad (1)$$

Based on the discharge curves, the discharge specific capacitance (C_s) of these hybrid supercapacitors were calculated by the following formula:

$$C_s = \frac{i \times \Delta t}{\Delta V \times m} \quad (2)$$

where i (A), ΔV (V), Δt (s) and m (g) are the discharge current, discharge potential range, discharge time consumed in the potential range ΔV, and the active mass of the single electrode, respectively. Based on the discharge curves in Figs. 7 and 8, the results of discharge specific capacitance for NiO/AC are listed in Table 1 according to formula (2).

Table 1
The first cycle and the 1000th cycle discharge specific capacitance for the NiO/AC supercapacitor with different nanoscale building blocks of NiO: (a) NiO hollow sphere composed of nanoparticles, (b) NiO sphere composed of nanoplates and (c) NiO sphere with a smooth surface.

Sample	Discharge specific capacitance (C_s) ($F\,g^{-1}$)	
	First cycle	1000th cycle
a	51.7	45.8
b	45.1	38.2
c	32.9	24.3

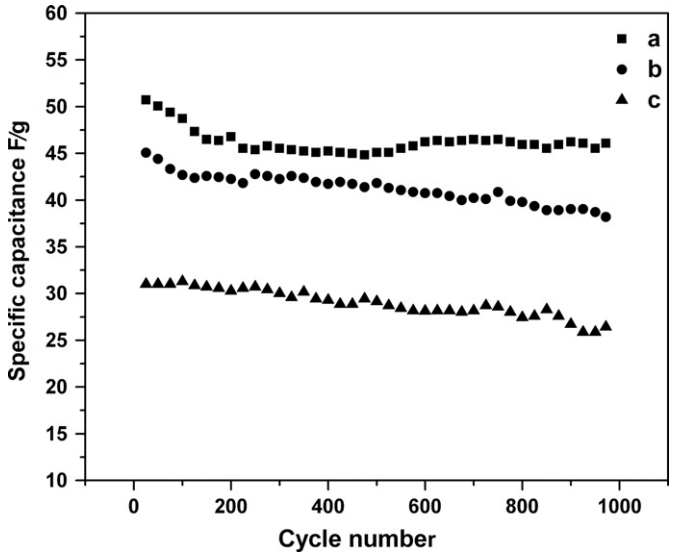

Fig. 9. Cycling performance of the NiO/AC hybrid capacitor at a current density of 100 mA/g in 6 mol/L KOH solution: (a) NiO hollow sphere composed of nanoparticles, (b) NiO sphere composed of nanoplates and (c) NiO sphere with a smooth surface.

Fig. 9 presents the cycling performance of the NiO/AC hybrid capacitor at a current density of 100 mA/g in 6 mol/L KOH solution. The data illustrate that these hybrid capacitors exhibited good capacity retention. As shown in Fig. 9 and Table 1, it is obvious that sample (a) exhibited better electrochemical performance and had the highest discharge specific capacity among the three samples, which may be attributed to its unique morphology with hollow sphere composed of nanoparticles and coarse surface. This kind of morphology should be in favor of the electrolyte inserting into or expelling out the oxide matrix and increase contact area between the electrolyte and the electrode material as a result of improving the utilization of the material [29]. It is also in favor of electrochemical reaction on the interface. Therefore NiO/AC supercapacitor with NiO hollow sphere composed of nanoparticles has a higher pseudo-capacitance. Sample (b) had the lower discharge specific capacity than that of sample (a), but higher than that of sample(c). The reason was as followed: In comparison with sample (c), sample (b) composed of NiO

nanoplates also had larger specific surface area and in favor of the contact with the electrolyte.

Based on these results, it is believed that the NiO with a hollow sphere composed of nanoparticles morphology is a good electrode material in supercapacitor field.

4. Conclusions

NiO hollow spheres obtained by calcining the $Ni(OH)_2$ precursor in a rapid combustion process. The results indicated that the glucose and the reaction temperature would affect the product morphology. NiO hollow spheres composed of nanoparticles are easy to form by adding glucose and keeping the reaction temperature at 140 °C under the hydrothermal conditions. Charge/discharge test results showed that the as-prepared NiO hollow spheres composed of nanoparticles exhibited a higher discharge capacity, which might serve as an ideal electrode material for supercapacitor due to the spherical hollow structure.

Acknowledgments

This work is financially supported by the National Natural Science Foundation of China (Grant 20701029). The authors are grateful to X.Y. Ji and X.Y. Zhang at Analytical and Testing Center in Sichuan University for XRD and SEM measurements.

References

[1] B. Lim, M.J. Jiang, J. Tao, P.H.C. Camargo, Y.M. Zhu, Y.N. Xia, Adv. Funct. Mater. 19 (2009) 189–200.
[2] N.N. Zhao, Y. Wei, N.J. Sun, Q. Chen, J.W. Bai, L.P. Zhou, Y. Qin, M.X. Li, L.M. Qi, Langmuir 24 (2008) 991–998.
[3] A. Tao, F. Kim, C. Hess, J. Goldberger, R.R. He, Y.G. Sun, Y.N. Xia, P.D. Yang, Nano Lett. 3 (2003) 1229–1233.
[4] T.L. Sounart, J. Liu, J.A. Voigt, J.W.P. Hsu, E.D. Spoerke, Z. Tian, Y.B. Jiang, Adv. Funct. Mater. 16 (2006) 335–344.
[5] Z.R. Tian, J. Liu, J.A. Voigt, B. Mckenzie, H.F. Xu, Angew. Chem. Int. Ed. 42 (2003) 413–417.
[6] T.Y. Kim, J.Y. Kim, S.H. Lee, H.W. Shim, S.H. Lee, E.K. Suh, K.S. Nahma, Synth. Met. 144 (2004) 61–68.
[7] D.S. Wang, R. Xu, X. Wang, Y.D. Li, Nanotechnology 17 (2006) 979–983.
[8] M.A. Gondal, M.N. Sayeed, Z. Seddigi, J. Hazard. Mater. 155 (2008) 83–89.
[9] P. Poizot, S. Laruelle, S. Grugeon, L. Dupont, J.M. Tarascon, Nature 407 (2000) 496–499.
[10] I. Hotovy, V. Rehacek, P. Siciliano, S. Capone, L. Spiess, Thin Solid Films 418 (2002) 9–15.
[11] F. Li, H.Y. Chen, C.M. Wang, K.A. Hu, J. Electroanal. Chem. 531 (2002) 53–60.
[12] G.A. Niklasson, C.G. Granqvist, J. Mater. Chem. 17 (2007) 127–156.
[13] S.G. Kim, S.P. Yoon, J. Han, S.W. Nam, T.H. Lim, I.H. Oh, S.A. Hong, Electrochim. Acta 49 (2004) 3081–3089.
[14] D.Y. Han, H.Y. Yang, C.B. Shen, X. Zhou, F.H. Wang, Powder Technol. 147 (2004) 113–116.
[15] C.K. Xu, K.Q. Hong, S. Liu, G.H. Wang, X.N. Zhao, J. Cryst. Growth 255 (2003) 308–312.
[16] Y.J. Zhan, C.R. Yin, C.L. Zheng, W.Z. Wang, G.H. Wang, J. Solid State Chem. 177 (2004) 2281–2284.
[17] H.A. Pang, Q.Y. Lu, Y.Z. Zhang, Y.C. Li, F. Gao, Nanoscale 2 (2010) 920–922.
[18] W.Z. Wang, Y.K. Liu, C.K. Xu, C.L. Zheng, G.H. Wang, Chem. Phys. Lett. 362 (2002) 119–122.
[19] Z.H. Liang, Y.J. Zhu, X.L. Hu, J. Phys. Chem. B 108 (2004) 3488–3491.
[20] S.A. Needham, G.X. Wang, H.K. Liu, J. Power Sources 159 (2006) 254–257.
[21] X.M. Ni, Y.F. Zhang, D.Y. Tian, H.G. Zheng, X.W. Wang, J. Cryst. Growth 306 (2007) 418–421.
[22] M. Zhang, G.J. Yan, Y.G. Hou, C.H. Wang, J. Solid State Chem. 182 (2009) 1206–1210.
[23] L. Liu, Y. Li, S.M. Yuan, M. Ge, M.M. Ren, C.S. Sun, Z. Zhou, J. Phys. Chem. C 114 (2010) 251–255.
[24] X.M. Sun, Y.D. Li, Angew. Chem. Int. Ed. 43 (2004) 3827–3831.
[25] X.L. Li, T.J. Lou, X.M. Sun, Y.D. Li, Inorg. Chem. 43 (2004) 5442–5449.
[26] M.M. Titirici, M. Antonietti, A. Thomas, Chem. Mater. 18 (2006) 3808–3812.
[27] L.P. Xu, Y.S. Ding, C.H. Chen, L.L. Zhao, C. Rimkus, R. Joesten, S.L. Suib, Chem. Mater. 20 (2008) 308–316.
[28] S. Venka, W. John, J. Electrochem Soc. 147 (2000) 880–885.
[29] C.C. Hu, T.W. Tsou, J. Power Sources 115 (2003) 179–186.